Materials Advances

ROYAL SOCIETY OF CHEMISTRY

PAPER

View Article Online
View Journal | View Issue

Cite this: *Mater. Adv.*, 2021, 2, 4277

Simultaneous improvement of kinetics and thermodynamics based on SrF_2 and SrF_2@Gr additives on hydrogen sorption in MgH_2†

Vivek Shukla,[a] Ashish Bhatnagar,[b] Satish K. Verma,[a] Anant P. Pandey,[a] Alok K. Vishwakarma,[a] Pankaj Srivastava,[c] T. P. Yadav[a] and O. N. Srivastava *[a]

Herein we describe and discuss the effect of significant advantages of the alkaline earth fluoride additive SrF_2 on the improvement of the kinetics, thermodynamics, and cyclability of the frontier hydrogen storage material MgH_2. Strontium fluoride, SrF_2, which has been used as an additive for the first time in the present study, has an elemental electronegativity difference of 3.04 (the highest amongst the fluorides) as compared to 2.38 for NbF_5, one of the best-known catalysts so far for MgH_2. Therefore, SrF_2 is highly ionic and will readily react with MgH_2, which is not only ionic but also has a polar covalent character. SrF_2 reacts with MgH_2 to yield magnesium fluoride (MgF_2) and strontium hydride (SrH_2) which act as catalysts. The present investigations have revealed that both (MgF_2 + SrH_2) and their graphene templated version, (MgF_2 + SrH_2)@Gr, work as better catalysts for MgH_2 than NbF_5. Thus the desorption of H_2 from ball-milled MgH_2 catalyzed by (MgF_2 + SrH_2) corresponds to 5.30 wt% in 15 min, and for (MgF_2 + SrH_2)@Gr the desorption is 6.01 wt% in 15 min at 290 °C. Also, the onset desorption temperatures for MgH_2 with (MgF_2 + SrH_2) and (MgF_2 + SrH_2)@Gr catalysts are 261 °C and 231 °C, respectively, which are 95 °C and 125 °C lower than that for ball-milled MgH_2. The H_2 absorption for (MgF_2 + SrH_2) catalyzed MgH_2 is found to be 6.00 wt% in 5 min at 290 °C. For (MgF_2 + SrH_2)@Gr catalyzed MgH_2 the hydrogen absorption is 6.16 wt% in 2 min at 290 °C. The change in desorption enthalpy for MgH_2–(MgF_2 + SrH_2)@Gr is 67.60 kJ mol^{-1} as compared to 74.84 kJ mol^{-1} for MgH_2–(MgF_2 + SrH_2). The storage capacity for MgH_2–(MgF_2 + SrH_2)@Gr remains ~6.00 wt% even after 15 cycles, which corresponds to excellent cyclability. A feasible catalytic mechanism arising from (MgF_2 + SrH_2) and (MgF_2 + SrH_2)@Gr catalysts on hydrogen sorption in MgH_2 has been proposed based on X-ray diffraction, Raman spectroscopy, Fourier transmission infrared spectroscopy, and transmission/scanning electron microscopic studies. The present study is the first of its type where absorption/desorption kinetics, thermodynamics, and cyclability for MgH_2 have all been improved by the use of the single additive SrF_2 and the derived catalyst MgF_2 + SrH_2.

Received 7th January 2021,
Accepted 7th February 2021

DOI: 10.1039/d1ma00012h

rsc.li/materials-advances

1 Introduction

Since the dawn of civilization, energy demands of human beings have been mostly met by fossil fuels.[1,2] Even if the availability of these can be assured until the end of this century, the deleterious effect which ensues due to the emission of CO_2 causing climate change may prohibit their use in the coming decades.[3,4] At present the CO_2 concentration in the atmosphere is 414 ppm.[5]

[a] *Hydrogen Energy Centre, Department of Physics, Banaras Hindu University, Varanasi-221005, India. E-mail: heponsphy@gmail.com, heponsphy.bhu@gmail.com; Tel: +91 05422368468*

[b] *Department of Physics and Materials Science and Engineering, Jaypee Institute of Information Technology, Noida, Sector-62, 201309, India*

[c] *Department of Chemistry, Banaras Hindu University, Varanasi-221005, India*

† Electronic supplementary information (ESI) available: Fig. S1: XRD spectra of (a) MgH_2, (b) MgH_2–SrF_2 and (c) MgH_2–SrF_2@Gr. Fig. S2: FTIR spectra of (a) MgH_2, (b) B.M. MgH_2–SrF_2, (c) Gr, (d) SrF_2@Gr and (e) MgH_2–SrF_2@Gr. Fig. S3: XRD spectra of (a) Mg–(MgF_2 + SrH_2) (1st dehydrogenation) and (b) Mg–SrF_2@Gr (1st dehydrogenation). Fig. S4: Scanning electron micrographs of (a) B.M. MgH_2–SrF_2, (b) 1st desorption of B.M. MgH_2–SrF_2 (Mg–(MgF_2 + SrH_2)@Gr), (c) B.M. MgH_2–SrF_2@Gr, and (d) after cycling of B.M. MgH_2–SrF_2@Gr (MgH_2–(MgF_2 + SrH_2)@Gr), (e) EDAX spectra after cycling of the MgH_2–(MgF_2 + SrH_2)@Gr sample and (f) elemental mapping after cycling of MgH_2–(MgF_2 + SrH_2)@Gr. Fig. S5: XRD spectra of (a) MgH_2–SrF_2@Gr and (b) after 15th adsorption run of Mg/MgH_2–(MgF_2 + SrH_2)@Gr. Fig. S6: DSC plot of ball milled MgH_2 for 25 h at different heating rates: (a) 5 °C min^{-1}, (b) 7 °C min^{-1} and (c) 10 °C min^{-1}. (ii) Kissinger plot for the calculation of activation energy. Fig. S7: FTIR spectra of (a) Mg–(SrH_2–MgF_2)@Gr (1st dehydrogenation), (b) Mg–(SrH_2–MgF_2)@Gr (after 14 cycles of dehydrogenation) and (c) MgH_2–(SrH_2–MgF_2)@Gr (after 15 cycles of rehydrogenation). See DOI: 10.1039/d1ma00012h

It has to be reduced to ~200 ppm (50% of current levels) so that by 2050 the temperature change of the environment is no more than 2 °C.[6] If climate change is not checked, the earth will become uninhabitable in a few decades. Another issue is the large gap between the supply and demand of energy. This continues to increase as the human population increases. The population of the earth will be 10 billion by the year 2050.[7] We need clean, abundant, and renewable energy that fulfills our energy demand for the long term. Decades of research have suggested that, out of various options, the most attractive candidate is hydrogen.[8] Hydrogen is produced from water, and it turns back to water upon high-temperature combustion, *e.g.*, IC engines or cold combustion in fuel cells. There has been a recent upsurge in research on the production, storage, and application of hydrogen. Out of these, the storage of hydrogen is the most crucial aspect, which cuts through production/distribution, safety, and application. The storage of hydrogen in the form of metal hydrides is the most efficient and safe mode of storage.[9,10] However, despite the intensive search for a hydride that fulfills the essential required limits, any viable hydride has not yet emerged. The limit required by the DOE for a solid-state storage system is 4.5 wt% and 36 g H_2 L^{-1}.[11] Such a system limit can be achieved only if the storage material shows a storage capacity higher than 4.5 wt% and 36 g L^{-1} of hydrogen. Research carried out in recent years suggests that MgH_2 may be such a storage material. It has a gravimetric storage capacity of 7.6 wt% and a volumetric storage capacity of 110 g H_2 L^{-1} and its storage is also reversible.[12] Mg is abundantly available on the earth's crust and in the sea. Thus it is a viable hydrogen material, but it has two hurdles related to high sorption temperature (~400 °C) and sluggish kinetics (<1 wt% min^{-1}).[13]

In the aforementioned background, many studies have been conducted to overcome the aforementioned difficulties associated with MgH_2. Partial success has been achieved in these efforts.[14] The most useful way in which efforts have been made to lower sorption temperature and improve kinetics is through the use of catalysts/additives. The most deployed catalysts are transition metals such as Ti, Fe, Co, Ni, Mn, Nb, V, and Zr, and their compounds.[15] Regarding the transition metal compounds, oxides and halides are potential candidates. Out of these, Nb_2O_5 and NbF_5 have received particular attention. However, it has been found that the addition of NbF_5 to MgH_2 leads to a better hydrogen sorption behavior than that of Nb_2O_5.[16,17] It has been found that, during cycling at higher temperature, Nb_2O_5 starts to get dissociated, leading to the formation of an increasing amount of MgO. In yet another study by Floriano *et al.*,[18] the superiority of NbF_5 over Nb_2O_5 in regard to the hydrogen desorption characteristics of MgH_2 has been elucidated. NbF_5 has been generally found to be a very effective catalyst for improving the hydrogen sorption characteristics of MgH_2.[17] The investigation carried out by Recham *et al.*[19] has shown that NbF_5 is a better additive than Nb_2O_5 as well as $NbCl_5$ for enhancing the hydrogen sorption kinetics. A detailed study on the effect of several transition metal halides, including NbF_5, has been conducted by Malka *et al.*[20,21] They have found the significant effect of NbF_5 on hydrogen sorption in MgH_2. Only ZrF_4 was found to be somewhat better than NbF_5.[16,17,19–23] These authors have also shown that, of the two halides NbF_5 and $NbCl_5$, the former is a better additive for MgH_2.

More recently, Santigo *et al.*[16] conducted a detailed study of the effect of NbF_5, which led to the formation of MgF_2 and $NbH_{0.9}$, on the hydrogen sorption kinetics in MgH_2. They have used two types of $NbH_{0.9}$ catalyst: one formed on milling MgH_2 with NbF_5 and the other separately synthesized. They have shown that NbF_5 exhibits excellent hydrogen sorption kinetics due to the homogeneous distribution of $NbH_{0.9}$ in the form of fine particles in MgH_2. However, they have found a significant decrease in the achievable hydrogen storage capacity. Contrary to the studies of Santiago *et al.*,[17] Jain *et al.*[23] have found that, when MgH_2 and MgF_2 are milled together, MgF_2 remains intact, does not dissociate and persists throughout the hydrogen sorption cycling. In these studies, (MgH_2 + MgF_2) has been shown to exhibit better hydrogen sorption than MgH_2 alone.

Fluorine has an electronegativity of 3.95, which is the highest out of all elements. Hence fluorides will be highly ionic and react readily with MgH_2, which is ionic but also has a polar covalent character.[24] As outlined above, so far, NbF_5 has been found to be the most suitable additive for MgH_2.[17,19] Here we have used a new fluoride SrF_2. This has a larger elemental electronegativity difference of 3.05 (Sr: 0.93 and F: 3.98) as compared to NbF_5, for which it is 2.38 (Nb: 1.60, F: 3.98). In fact, SrF_2 has the largest electronegativity difference out of all non-radioactive fluorides. We have shown that SrF_2 works as a significantly better additive for hydrogen sorption in MgH_2. The additive SrF_2 reacts with MgH_2 while it is heated for dehydrogenation and produces two compounds MgF_2 and SrH_2. These remain stable and are present throughout the hydrogen sorption cycling and act as catalysts. They lead to the improvement of hydrogen sorption kinetics and thermodynamics. As a further factor for the improvement of hydrogen sorption in MgH_2, we have used graphene templation of SrF_2 and (MgF_2 + SrH_2). (MgF_2 + SrH_2) and (MgF_2 + SrH_2)@Gr catalyzed MgH_2 show onset desorption temperatures of 261 °C and 231 °C, respectively, which are 95 °C and 125 °C lower than that of ball-milled MgH_2, for which it is 356 °C. MgH_2 catalyzed by (MgF_2 + SrH_2)@Gr shows superior dehydrogenation kinetics. It desorbs 6.01 wt% in 15 min at 290 °C. It also shows better rehydrogenation kinetics by absorbing 6.16 wt% in 2 min at 290 °C and 18 atm H_2 pressure. The storage capacity remains ~6 wt% even up to 15 cycles. Thus MgH_2–(MgF_2 + SrH_2)Gr shows excellent cyclability. Therefore, in contrast to earlier studies with NbF_5,[16] the storage capacity remains intact during cycling with the SrF_2@Gr additive. The change in desorption enthalpy for MgH_2–7 wt% (MgF_2 + SrH_2) and MgH_2–7 wt% (MgF_2 + SrH_2)@Gr samples was found to be 74.84 kJ mol^{-1} and 67.60 kJ mol^{-1}, respectively. These are significantly lower than the desorption enthalpy of MgH_2, which is 80.66 kJ mol^{-1}. It may be mentioned that earlier studies[16] employing the MgF_2–$NbH_{0.9}$ catalyst do not suggest any improvement in enthalpy (thermodynamics). Also, in these studies, the storage capacity significantly decreases on cycling.[16] The present catalysts (MgF_2 + SrH_2) and (MgF_2 + SrH_2)@Gr lead to

the improvement of both the hydrogen sorption kinetics and thermodynamics of hydrogen sorption in MgH_2. The present study forms one of the few cases and, to the best of our knowledge, the first case for a fluoride–hydride catalyst which leads to the improvement of all hydrogen sorption characteristics, namely, kinetics, thermodynamics and cyclability.

2 Experimental section

2.1. Synthesis of SrF_2@Gr

Strontium fluoride (Alfa Aesar) was ball-milled at 180 rpm for 24 hours with a ball-to-powder ratio of 50 : 1 under 5 atm hydrogen pressure before further use. High quality graphene has been routinely produced in our laboratory.[25] SrF_2 was templated on graphene using the following steps. Firstly, sodium dodecyl sulfate (SDS) (0.004 g), Gr (0.0145 g), and dimethylformamide (DMF) ($\sim$50 mL) were mixed. Then the resultant solution was mixed homogeneously by using an ultrasonicator at 20 kHz for 2 hours. Finally, 0.582 g of the SrF_2 base material was added to the above solution, followed by sonication at room temperature until a homogeneous dark solution was formed. The material so obtained was dried overnight in a vacuum at 60 °C, collected, and characterized. The resulting material, as confirmed by XRD and Raman spectroscopy, corresponds to SrF_2@Gr. This was further used as the additive for hydrogen sorption in Mg/MgH_2. Our previous studies have shown the synthesis protocol and detailed procedure of graphene templation.[26–28]

2.2. Synthesis of MgH_2 admixed with graphene templated SrF_2 (SrF_2@Gr)

MgH_2 (99.99%) was purchased from Nanoshel (UK). 7 wt% of SrF_2@Gr was added to the pure MgH_2 sample. MgH_2–SrF_2@Gr was synthesized by mechanical milling of SrF_2@Gr with MgH_2. The mixture was ball-milled at 180 rpm for 25 hours with a ball-to-powder ratio of 50 : 1 (by weight) using a Retsch PM 400 planetary ball miller. For brevity, instead of writing 7 wt% SrF_2, we will henceforth mention it simply as SrF_2. The quantity 7 wt% will be implied. Also, all samples including Mg alone were prepared through ball milling. Hence, we will not add the suffix B.M. to the samples and it is taken to be implied. The concentration of the additive (SrF_2@Gr) was taken to be 7 wt% of MgH_2. It was found that 7 wt% of the additive (SrF_2@Gr) is optimum (in terms of desorption temperature and hydrogen storage capacity) for hydrogen sorption in Mg/MgH_2. To avoid contamination from air during ball milling, the vial containing materials was filled with hydrogen gas with 5 atm pressure. All samples were transferred and loaded inside a N_2 filled glove box (MBRAUN MB-10 compact) with O_2 and H_2O levels $<$1 ppm.

2.3. Characterization techniques

For the structural characterization of the prepared samples, XRD data were collected with a Panalytical Empyrean X-ray diffractometer equipped with an area detector (256 $\times$ 256 pixels) at 0.02 °C step size in 2θ range from 10°–110° with CuKα radiation (λ = 1.5415 Å) operated at 40 kV, 40 mA. All the samples were wholly covered with parafilm to prevent the sample reactions from atmospheric contamination during XRD. The microstructures of the samples were studied by transmission electron microscopy (TEM), and selected area electron diffraction (SAED) patterns using TEM: TECNAI 20 G^2 at an accelerating voltage of 200 kV. The surface morphology and energy dispersive X-ray analysis (EDAX) with the color mapping of elements of as-prepared samples was done by using a scanning electron microscope (SEM): FEI Quanta 200 with operating voltage 25 kV in a high vacuum ($\sim 10^{-5}$ torr). Fourier transform infrared (FTIR) spectroscopy was carried out using a PerkinElmer (Spectrum 100) spectrometer in transmission mode with wavenumbers ranging from the mid-infrared region (400–4000 cm^{-1}).

The dehydrogenation properties of the as-prepared samples were analyzed by temperature-programmed desorption (TPD) at a heating rate of 3 °C min^{-1}. TPD analysis of the catalyzed and uncatalyzed MgH_2 was started under vacuum (10^{-3} torr) using dynamic heating conditions with a precision of $\pm$0.2 °C. Rehydrogenation kinetics was measured in the soak mode at 290 °C under 15 atm pressure. Dehydrogenation kinetics was measured using the release mode of the instrument at 290 °C under 1 atm pressure. All the de/rehydrogenation measurements were performed using an automated two-channel volumetric Sievert type apparatus supplied by Advanced Materials Corporation Pittsburgh, USA.

3 Results and discussion

3.1 (a) Synthesis of SrF_2@Gr

In order to verify the templation of the additive over graphene, transmission electron microscopy analysis of the SrF_2@Gr sample was performed. Fig. 1 shows a representative TEM micrograph of the templated version of nano-SrF_2 over graphene. Fig. 1(a) shows a representative TEM micrograph of graphene. The expected wrinkled microstructure of graphene is visible. The SAED pattern of graphene shows (002) and (110) graphitic peaks (Fig. 1(b)). Indexing of the diffraction pattern by a diffraction ring profiler can be seen in Fig. 1(c). Fig. 1(d) shows the TEM micrograph of SrF_2@Gr, which confirms the templation of SrF_2 over graphene. Fig. 1(c) and (f) has been again indexed with a diffraction ring profiler. It may be noted that, during the TEM analysis, the SrF_2 samples templated on graphene were taken out and then inserted again. As verified by several such runs, the SrF_2 particles remained on graphene and did not fall off. This showed that the SrF_2 particles are anchored on graphene (Fig. 1(d)). Fig. 1(f) has been again indexed with a diffraction ring profiler.

3.1 (b) Characterization of MgH_2 admixed with SrF_2 templated on graphene (MgH_2–SrF_2@Gr)

A quantity of 7 wt% of SrF_2 was added to MgH_2. The concentrations of the additives SrF_2 and SrF_2@Gr were found to be

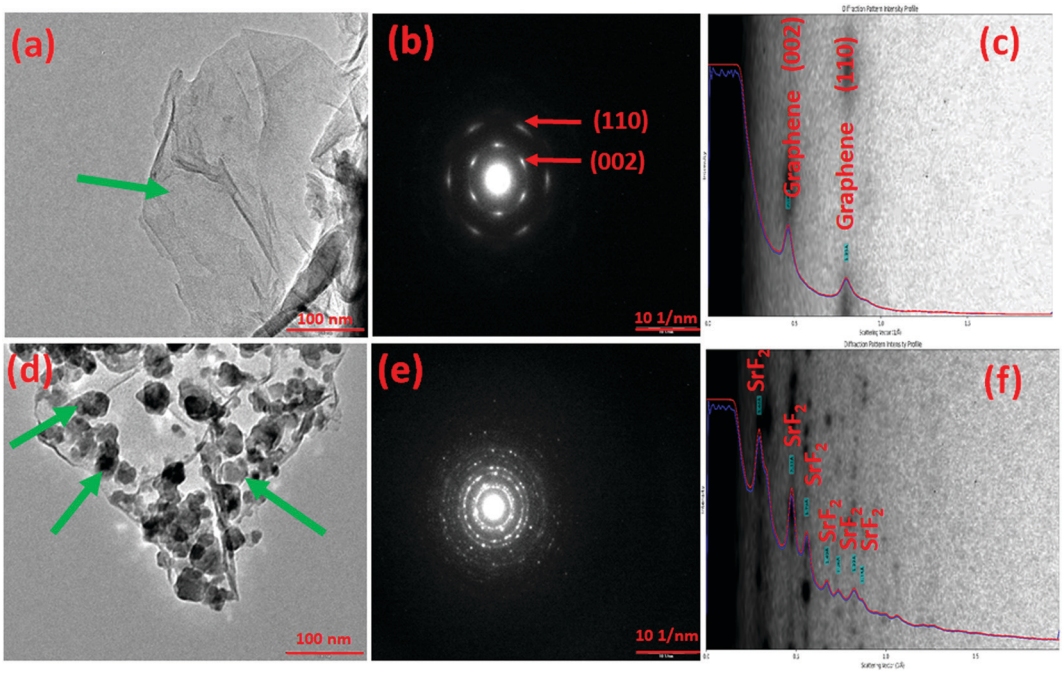

Fig. 1 TEM micrographs of (a) graphene, (b) SAED pattern of graphene, (c) diffraction ring profiler indexing of graphene, (d) SrF_2@Gr, (e) SAED pattern of SrF_2@Gr, and (f) diffraction ring profiler indexing of SrF_2@Gr.

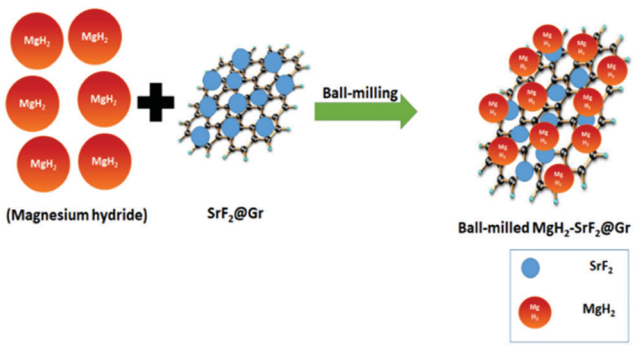

Fig. 2 Schematic diagram for MgH_2 admixed with SrF_2 templated on graphene (MgH_2–SrF_2@Gr).

optimum for catalyzing MgH_2. A schematic diagram of the templation of SrF_2 on Gr is shown in Fig. 2.

To check the obtained XRD data with the standard crystallographic data and phases present in the sample, we performed multiphase Le Bail fitting of the XRD patterns using JANA software.[26] The XRD data (2θ = 20–80°) for MgH_2 and the admixed version of MgH_2 samples are also shown in Fig. S1(i) (ESI†). Fig. 3(a)–(c) show the XRD fitting (difference plot with model and experimental data) of MgH_2 and the admixed version of the MgH_2 sample. The peak from 20° to 25° has been left intentionally as 2θ = 21.16° and 23.50°, which corresponds to the peak of the parafilm, which is used as a cover on the XRD holder to avoid contamination of the sample from air and moisture. Fig. 3(a)–(c) and Fig. S1(a–c) (ESI†) show the XRD patterns of the ball-milled MgH_2 additive with SrF_2 and SrF_2@Gr. Fig. 3(a) shows the XRD pattern of the ball-milled MgH_2, where all the XRD peaks tally with the known XRD peaks of β-MgH_2. No evidence of high-pressure γ-MgH_2 has been found. Fig. 3(b) shows the XRD pattern of SrF_2 admixed with MgH_2, where the phases of SrF_2 and MgH_2 have been indexed in XRD. Fig. 3(c) shows the XRD pattern of MgH_2 admixed with SrF_2 templated on graphene (SrF_2@Gr). The phases of MgH_2 and SrF_2 can be clearly seen in the XRD pattern. The analysis of the XRD pattern of SrF_2@Gr added MgH_2 indicates that all the peaks are of MgH_2 and SrF_2 NPs. The Gr peaks are very weak and broad (Fig. 1). They get obliterated in the background and with peaks of MgH_2 and SrF_2.

Fig. 4 shows the Raman spectra of graphene (Gr) and the SrF_2@Gr added MgH_2 sample. Fig. 4(a) shows the Raman spectrum of graphene. As is known, the G band corresponds to the in-plane vibration of sp^2 hybridized carbon. The D band represents the vibrations of carbon atoms at defect sites, including the carbon at the edge atoms forming dangling bonds.[28,29] The D and G bands together with the 2D band can be seen in Fig. 4(a). Fig. 4(b) shows the Raman spectrum of the ball-milled SrF_2@Gr with added MgH_2 sample. The D and G bands are present together as a 2D band. It can be said that the Raman spectra helps to identify the nanostructured carbon catalyst, which has not been clearly revealed from the XRD results. If we compare Fig. 4(a) and (b), the I_D/I_G ratio is less than one ($I_D/I_G < 1$) for graphene and greater than one ($I_D/I_G > 1$) for SrF_2@Gr with added MgH_2. This may be due to the creation of defects during ball milling due to which the intensity of the D band is enhanced. This reveals the fact that there is an interaction between Gr and SrF_2, which may lead to the displacement of carbon atoms in graphene. The TEM micrographs shown in Fig. 1(a)–(f) show SrF_2 nanoparticles located on graphene (Gr). Even when the sample (SrF_2@Gr) was taken out from the TEM and inserted again, there was no

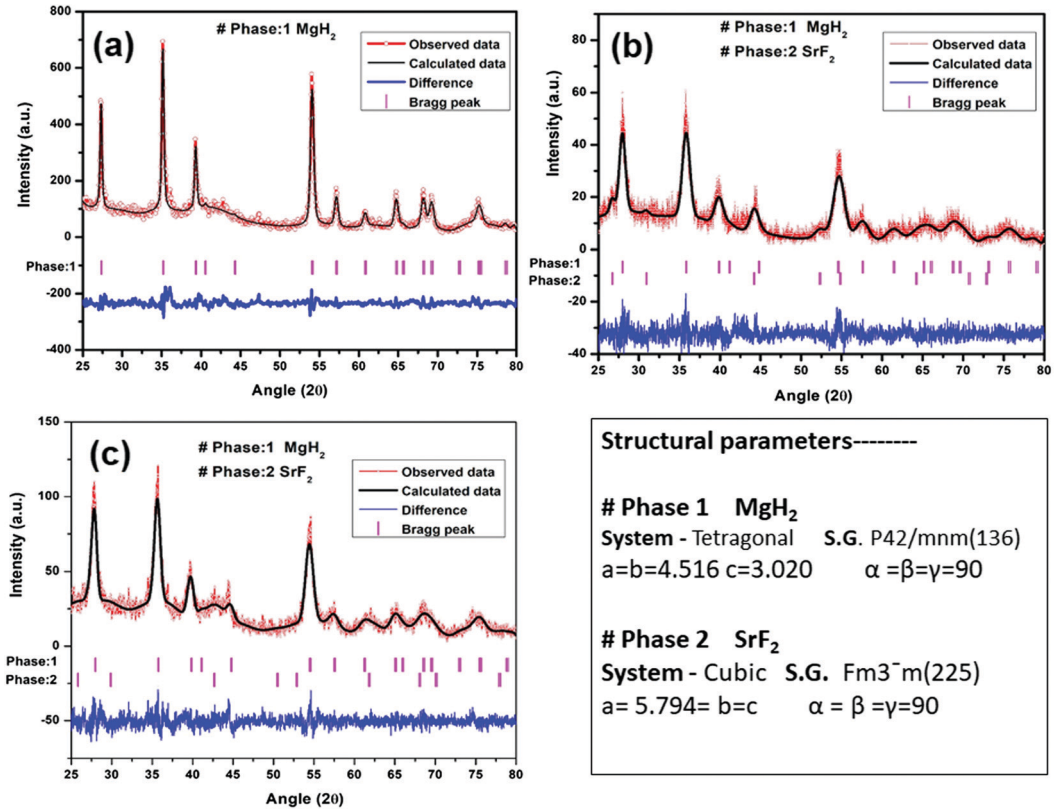

Fig. 3 XRD patterns of MgH_2 admixed with SrF_2 and SrF_2 templated on graphene (SrF_2@Gr) with Le Bail fitting using Jana software: (a) MgH_2, (b) MgH_2–SrF_2, and (c) MgH_2–SrF_2@Gr.

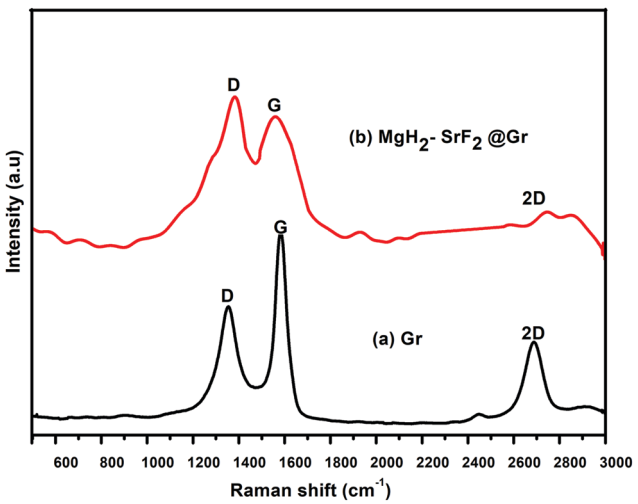

Fig. 4 Raman spectra of (a) graphene (Gr) and (b) MgH_2–SrF_2@Gr.

displacement of SrF_2 nanoparticles. This shows that SrF_2 (NPs) are anchored on graphene. Experiments covering several de/rehydrogenation samples have shown that SrF_2 (NPs) remain anchored on graphene.

3.2 Hydrogen sorption studies

3.2 (a) Formation of MgF_2 and SrH_2. It may be mentioned that, in previous studies on fluoride as an additive for MgH_2, it has been found that on heating for dehydrogenation of MgH_2 the fluoride generally dissociates yielding new compounds.[16,17,19] On the other hand, there have been some studies where the fluoride additive/catalyst remains intact.[23] In order to check the status of SrF_2 on heating with MgH_2, for dehydrogenation, the XRD patterns of the dehydrogenated samples were taken. The dehydrogenation was done at 290 °C at which complete dehydrogenation was found to take place. Fig. 5(a) and (b) or Fig. S3(a) and (b) (ESI†) show the representative XRD patterns of dehydrogenated MgH_2–SrF_2 and MgH_2–SrF_2@Gr, respectively. Indexing the XRD peaks revealed that, on dehydrogenation where heating at high temperature (~300 °C) is involved, SrF_2 was no longer present. Instead two products MgF_2 and SrH_2 were formed. Studies involving several dehydrogenation runs showed that, after dehydrogenation of MgH_2–SrF_2 and MgH_2–SrF_2@Gr, MgF_2 and SrH_2 together with Mg are invariably present. For the graphene templated version the formed products will be located on Gr. It may be pointed out that the reaction of MgH_2 and SrF_2 is not expected to be instantaneous. There is every possibility of formation of the metastable phase $Sr(F_xH_{2-x})$ as reported by Santiago *et al.*[16] This metastable phase $Sr(F_xH_{2-x})$ then dissociates so as to form SrH_2 (and the other associated compound MgF_2). However, due to the low concentration of SrH_2 the trace of $Sr(F_xH_{2-x})$ could not be found in the present study.

The reaction of MgH_2 and SrF_2 can be described as follows. (1) When MgH_2 reacts with SrF_2 (molar ratio 1 : 1) it forms

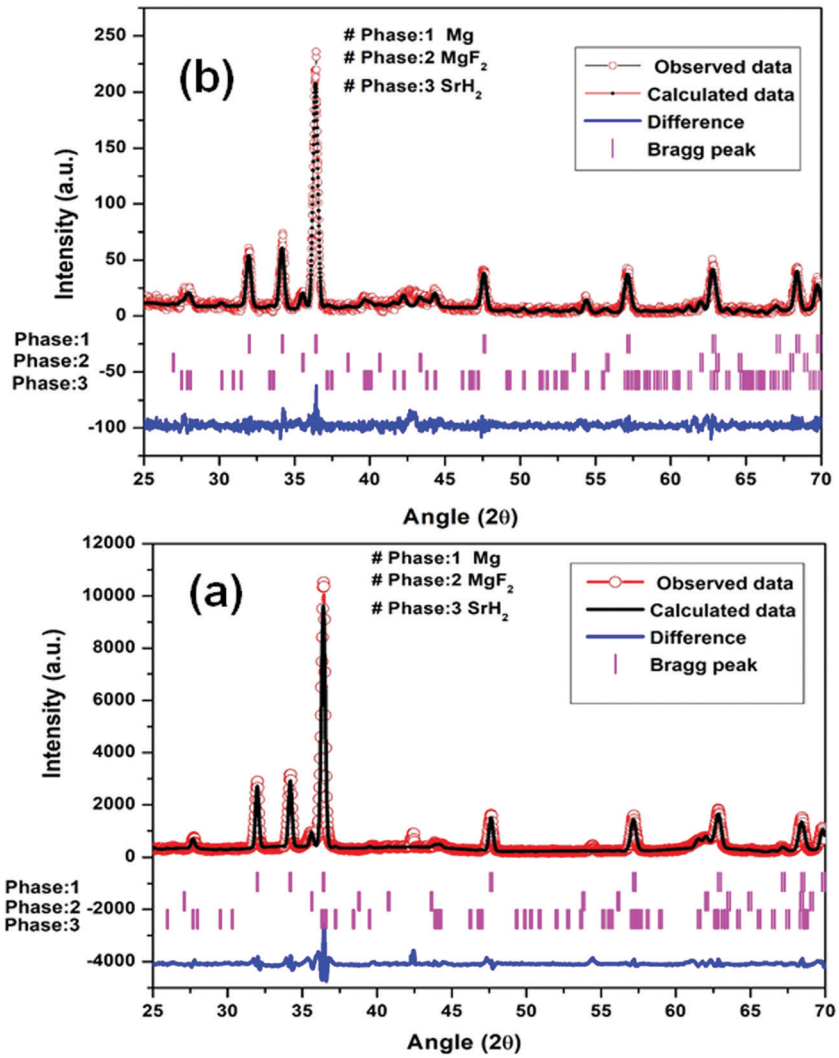

Fig. 5 Le Bail fitting of XRD patterns using JANA software at different steps: (a) Mg–(MgF_2 + SrH_2) (1st dehydrogenation) and (b) Mg–(MgF_2 + SrH_2)@Gr (1st dehydrogenation).

$$MgH_2 + SrF_2 \rightarrow MgF_2 + SrH_2 \quad (1)$$

(2) When MgH_2 desorbs to Mg, it forms

$$MgH_2 \rightarrow Mg + H_2 \quad (2)$$

Attempts were made to determine the stage of dehydrogenation at which the products MgF_2 and SrH_2 were formed. It was found that, when the peak desorption temperature (Fig. 6(ii)) was reached, the conversion of (MgH_2 + SrF_2) to (MgF_2 + SrH_2) invariably takes place. It may be pointed out that, as is known, the fluoride additive lowers the desorption temperature for all Mg based storage materials.[21] Thus it may be considered that initially SrF_2 may decrease the desorption temperature of MgH_2. However, once the reaction starts MgH_2 + SrF_2 is converted into MgF_2 + SrH_2 corresponding to the quantity of the additive taken. This conversion is completed when the peak desorption temperature is reached. Similar is the case for ball-milled MgH_2–SrF_2@Gr.

It may be pointed out that, after the first dehydrogenation reaction, besides Mg, the products which result, namely, MgF_2 and SrH_2, are present in all absorption/desorption runs. Further hydrogen (absorption/desorption) runs showed a significant improvement in kinetics, thermodynamics, activation energy and cyclability. Apparently the improvements in hydrogen sorption in MgH_2 are due to (MgF_2 + SrH_2) and (MgF_2 + SrH_2)@Gr which act as catalysts.

We now proceed to describe and discuss hydrogen sorption studies in (MgF_2 + SrH_2) and (MgF_2 + SrH_2)@Gr catalyzed MgH_2.

3.2 (b) Temperature programmed desorption (TPD). In order to estimate the onset of desorption for (MgF_2 + SrH_2) catalyzed MgH_2, the hydrogenation of the product, namely, Mg (MgF_2 and SrH_2), was conducted at 300 °C and 20 atm hydrogen pressure for 4 hours. The samples were brought to room temperature. After this temperature programmed desorption was carried out as follows.

The TPD of MgH_2 catalyzed by (MgF_2 + SrH_2) and also (MgF_2 + SrH_2)@Gr was conducted at a heating rate of 3 °C min^{-1}. Fig. 6(i, a–c) show the TPD of ball-milled MgH_2 and the catalyzed versions of MgH_2. Fig. 6(i-a) showing the TPD of the ball-milled MgH_2 sample exhibits the onset of desorption at

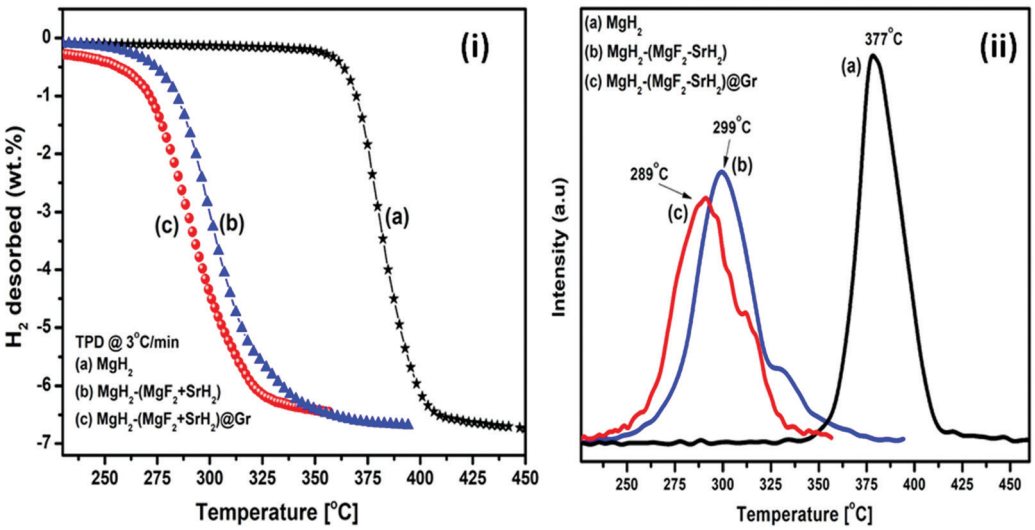

Fig. 6 (i) TPD of MgH_2 catalyzed by (a) MgH_2, (b) MgH_2–(MgF_2 + SrH_2), (c) MgH_2–(MgF_2 + SrH_2)@Gr and (ii) TPD (peak intensity *vs.* temperature) of (a) MgH_2, (b) MgH_2–(MgF_2 + SrH_2), and (c) MgH_2–(MgF_2 + SrH_2)@Gr.

356 °C. The complete dehydrogenation of MgH_2 has been found at 418 °C with a desorption capacity of 6.60 wt%. The onset desorption temperature for MgH_2 catalyzed by (MgF_2 + SrH_2) has been found at 261 °C. The complete dehydrogenation takes place at 351 °C showing a storage capacity of 6.41 wt%. The onset desorption temperature for (MgF_2 + SrH_2)@Gr catalyzed MgH_2 has been found to be 231 °C. Nearly 3.41 wt% of hydrogen is desorbed at the temperature of 292 °C, showing a complete dehydrogenation capacity of 6.32 wt% is obtained at 320 °C. The onset desorption temperature for (MgF_2 + SrH_2)@Gr catalyzed MgH_2 has been found to be lower by 125 °C and 30 °C than those for MgH_2 and (MgF_2 + SrH_2) catalyzed MgH_2, respectively. Thus it can be said that the hydrogen sorption characteristics of (MgF_2 + SrH_2)@Gr catalyzed MgH_2 are superior to those of (MgF_2 + SrH_2) alone. It may be pointed out that the present onset desorption temperature of 231 °C is one of the lowest onset temperatures observed for MgH_2 catalyzed by various catalysts.[23,26–28,30–35]

3.2 (c) De/rehydrogenation kinetics. The rehydrogenation/dehydrogenation kinetics profiles are shown in Fig. 7(i) and (ii), respectively. Fig. 7(i, a–c) show the rehydrogenation kinetics of MgH_2, MgH_2–(MgF_2 + SrH_2), and MgH_2–(MgF_2 + SrH_2)@Gr samples, respectively. The rehydrogenation kinetics was measured at 290 °C and 1.8 MPa H_2 pressure. In the present inverstigation, invariably ball-milled samples of MgH_2, MgH_2-(MgF_2 + SrH_2) were used, we will henceforth, for brevity, write MgH_2, MgH_2-(MgF_2 + SrH_2) instead of B.M. MgH_2, B.M. MgH_2-(MgF_2 + SrH_2). Also for all samples the catalyst quantity

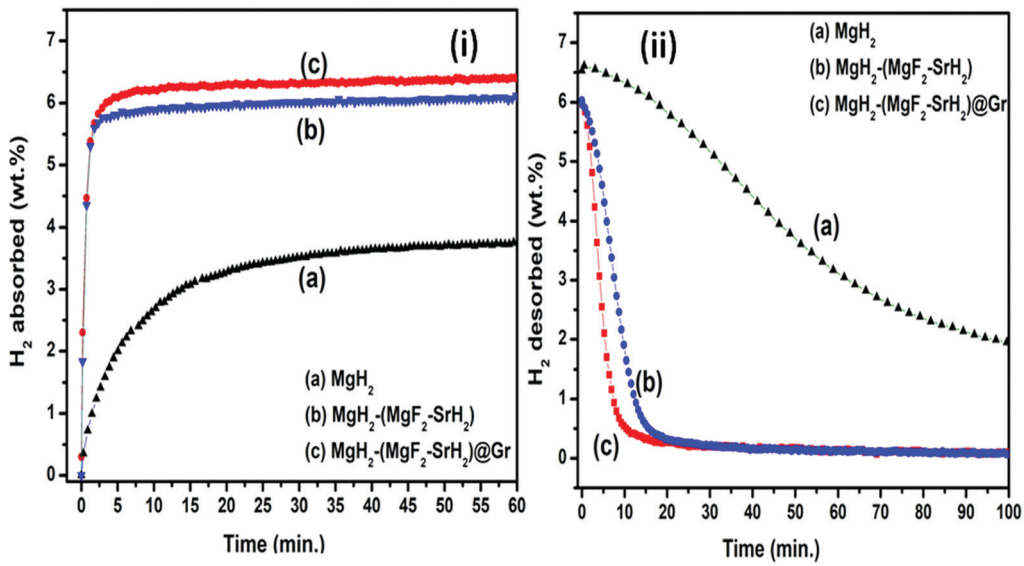

Fig. 7 De/rehydrogenation kinetics profile. (i) Rehydrogenation kinetics curve at 290 °C and 1.8 MPa H_2 pressure: (a) MgH_2, (b) MgH_2–(MgF_2 + SrH_2), and (c) MgH_2–(MgF_2 + SrH_2)@Gr. (ii) Dehydrogenation kinetics curve at 290 °C and 0.1 MPa H_2 pressure: (a) MgH_2, (b) MgH_2–(MgF_2 + SrH_2), and (c) MgH_2–(MgF_2 + SrH_2)@Gr.

Table 1 Comparison of rehydrogenation kinetics at ~300 °C in 2 min with different metal fluorides

S. no.	Catalyst/additive used	Rehydrogenation kinetics in 2 min (wt%)	Ref.
1.	TiF_3	4.5	32
2.	VF_4	3.5	32
3.	NbF_5	4.5	17 and 32
4.	NiF_2	3.2	32
5.	ZrF_4	3.6	32
6.	CrF_2	3.1	32
7.	FeF_2	3.2	32
8.	CeF_3	4.6	33
9.	LaF_3	4.5	33
10.	MgF_2	3.0	23
11.	MgF_2 + SrH_2	5.9 (T_{abs} −290 °C)	Present study
12.	MgF_2 + SrH_2@Gr	6.2 (T_{abs} −290 °C)	Present study

of 7 wt.% has been used. In view of this the prefix: corresponding to 7 wt.% for the catalysts will be taken as implied. The rehydrogenation kinetics of the MgH_2 sample is slow (Fig. 7(i-a)), *i.e.*, it only absorbs 2.02 wt% in 5 min and 3.05 wt% in 15 min. Nearly 3.76 wt% of H_2 is absorbed in 20 min. Fig. 7(i-b) show the rehydrogenation kinetics of the MgH_2–(MgF_2 + SrH_2) sample, the rehydrogenation kinetics of the catalyst system (MgF_2 + SrH_2) is improved, and it can absorb 5.90 wt% in 2 min and 6.00 wt% in 5 min. Fig. 7(i-c) show the rehydrogenation kinetics of (MgF_2 + SrH_2)@Gr catalyzed MgH_2 where very fast kinetics takes place. The MgH_2–(MgF_2 + SrH_2)@Gr adsorbs 6.16 wt% in 2 min. The rehydrogenation kinetics of the MgH_2–(MgF_2 + SrH_2)@Gr sample shows better rehydrogenation compared to our recent and other studies.[23,26–28,30–35] Rehydrogenation of 5.90 wt% and 6.20 wt% for MgH_2–(MgF_2 + SrH_2) and MgH_2–(MgF_2 + SrH_2)@Gr, respectively, in 2 min represents one of the fastest H_2 absorption processes for Mg. A comparison of the absorption kinetics for MgH_2 with different catalysts/additive is shown in Table 1.

Fig. 7(ii, a–c) show the dehydrogenation kinetics of MgH_2, MgH_2–(MgF_2 + SrH_2), and MgH_2–(MgF_2 + SrH_2@Gr) samples, respectively. The dehydrogenation kinetics was performed at 290 °C and 0.1 MPa H_2 pressure. Fig. 7(ii-a) shows the dehydrogenation kinetics profile of the MgH_2 sample. As shown in Fig. 7(ii-a), the MgH_2 sample desorbs 0.19 wt% in 5 min and 0.56 wt% in 15 min. The desorption of 4.69 wt% of H_2 has been observed in 100 min. Fig. 7(ii-b) shows the dehydrogenation kinetics of the MgH_2-(MgF_2 + SrH_2) sample, the dehydrogenation kinetics for this sample is improved, and it desorbs 1.68 wt% in 5 min and 5.59 wt% in 15 min. Fig. 7(ii-c) shows the dehydrogenation kinetics of (MgH_2)–(MgF_2 + SrH_2)@Gr. The MgH_2 sample with the graphene templated catalyst (MgF_2 + SrH_2) desorbs 4.08 wt% in 5 min and 6.01 wt% in 15 min. MgH_2–(MgF_2 + SrH_2)@Gr desorbs 6.11 wt% in 25 min. Thus the dehydrogenation kinetics of MgH_2 catalyzed by the (MgF_2 + SrH_2)@Gr sample shows better dehydrogenation compared to our recent and other studies.[23,26–28,30–35]

3.2 (d) Cycling stability. To check the cycling stability of (MgF_2 + SrH_2) and (MgF_2 + SrH_2)@Gr catalyzed MgH_2 samples, we performed continuous de/rehydrogenation experiments at 290 °C as shown in Fig. 8. The dehydrogenation of the optimum

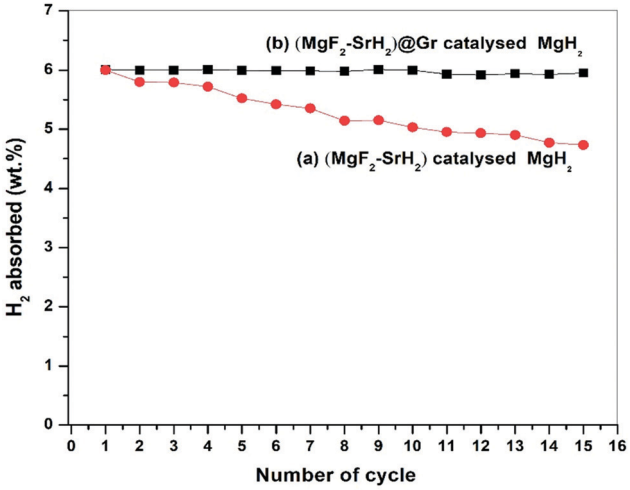

Fig. 8 Cycling stability up to 15 cycles of (a) (MgF_2 + SrH_2) catalysed MgH_2 and (b) (MgF_2 + SrH_2)@Gr catalysed MgH_2.

material MgH_2–(MgF_2 + SrH_2)@Gr was performed at 290 °C and 0.1 MPa H_2 pressure. The rehydrogenation was carried out at 290 °C and 1.8 MPa H_2 pressure. In order to compare the cycling stability of MgH_2–(MgF_2 + SrH_2) and MgH_2–(MgF_2 + SrH_2)@Gr, repeated de/rehydrogenation experiments were performed up to 15 cycles. The MgH_2–(MgF_2 + SrH_2) sample in the first cycle absorbs 6.01 wt% and 5.72 wt% in the 10th cycle. In the 15th cycle, the absorption capacity of the MgH_2–(MgF_2 + SrH_2) sample is lowered, reaching 4.73 wt%. However, with the graphene templated version, the cycling stability of the sample is improved. The MgH_2–(MgF_2 + SrH_2)@Gr sample absorbs 6.12 wt% in the first cycle and about the same quantity after the 15th cycle (even after 15 cycles it remains ~6.10 wt%). Thus there is almost no decrement of the storage capacity on cycling. The remarkable cycling stability is due to graphene on which the catalyzed particles are anchored. Similar to the case of SrF_2 templated on graphene (Section 3.1(a)), TEM studies show that MgF_2 and SrH_2 remain templated and hence anchored on graphene. Thus there is no agglomeration of MgF_2 and SrH_2.

3.2 (e) Differential scanning calorimetry for the calculation of activation energy. To understand the improvement in dehydrogenation kinetics, the lowering of the activation energy barrier in the presence of the catalyst (MgF_2 + SrH_2)@Gr in MgH_2 was determined by differential scanning calorimetry. The DSC was performed under nitrogen flow (20 mL min^{-1}) at heating rates of 5 °C min^{-1}, 7 °C min^{-1}, and 10 °C min^{-1}.

To find the activation energy using the Kissinger equation[36,37] the peak desorption temperature at different heating rates was used.

$$\ln(\beta/T_p^2) = (-E_a/RT_p) + \ln(k_o) \quad (3)$$

where T_p is the corresponding peak desorption temperature and β is the heating rate. The slope obtained from the plot between $\ln(\beta/T_p^2)$ and $1000/T_p$ is used for calculating the desorption activation energy and is shown in Fig. 10(ii). The activation energy for (MgF_2 + SrH_2)@Gr is 79.92 kJ mol^{-1}. This signifies the better

catalytic activity of (MgF_2 + SrH_2)@Gr over MgH_2 nanoparticles. The activation energy of 79.92 kJ mol^{-1} implies that we have to apply 79.92 kJ mol^{-1} energy to overcome the energy barrier for the conversion of MgH_2 into Mg in the case of MgH_2 catalyzed by (MgF_2 + SrH_2)@Gr. However, the activation energy of the ball-milled MgH_2 (25 hours) is 160.06 kJ mol^{-1} as shown in Fig. S6 (ESI†). This activation energy (79.92 kJ mol^{-1}) is significantly lower as compared to other catalysts, *e.g.* 130 kJ mol^{-1},[38] 131 kJ mol^{-1},[39] and 111 kJ mol^{-1}.[40]

3.2 (f) Thermodynamic stability. To understand the thermodynamic stability of MgH_2–(MgF_2 + SrH_2) and MgH_2–(MgF_2 + SrH_2)@Gr, enthalpy changes were evaluated and compared. The change in enthalpy for the de/rehydrogenation was calculated by pressure composition isotherm (PCI). Representative PCI curves for different samples are shown in Fig. 11(i) and (ii).

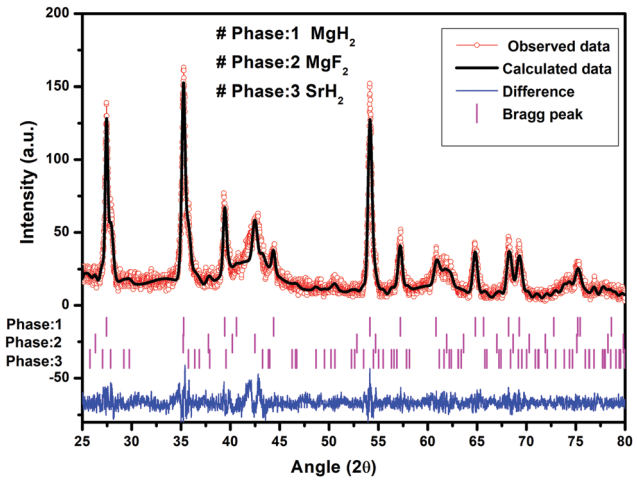

Fig. 9 Le Bail fitting of the XRD pattern using JANA software after 15 cycles of H_2 de/rehydrogenation of MgH_2–(MgF_2 + SrH_2)@Gr.

The PCI was carried out at 282 °C, 302 °C, and 320 °C for the MgH_2–(MgF_2 + SrH_2) sample to calculate the change in the enthalpy of the sample. The enthalpy change in the process of de/re-rehydrogenation has been evaluated using the van't Hoff plot. The enthalpy change for the dehydrogenation of MgH_2/Mg with (MgF_2 + SrH_2) has been found to be 74.84 kJ mol^{-1} (Fig. 11(i, a and b)). However, the enthalpy change for rehydrogenation (Mg to MgH_2) with (MgF_2 + SrH_2) is 67.99 kJ mol^{-1} (Fig. 11(i, c and d)). In order to calculate the enthalpy change of MgH_2–(MgF_2 + SrH_2)@Gr, PCI was performed at 288 °C, 311 °C, and 321 °C. The enthalpy change for the dehydrogenation of MgH_2–(MgF_2 + SrH_2)@Gr has been found to be 67.60 kJ mol^{-1} (Fig. 11(ii, a and b)). However, the enthalpy change for the rehydrogenation of MgH_2–(MgF_2 + SrH_2)@Gr is 61.54 kJ mol^{-1} (Fig. 11(ii, c and d)). Thus the desorption enthalpy change for MgH_2–(MgF_2 + SrH_2)@Gr has been found to be lower by 7.42 kJ mol^{-1} as compared to MgH_2–(MgF_2 + SrH_2). The change in the enthalpy of MgH_2/Mg has been found to be superior to those reported in several other studies.[26,27,31–35] Thus it can be said that the graphene templation of (MgF_2 + SrH_2) plays a vital role in promoting the whole reaction.

4 Proposed mechanism for the hydrogen sorption of MgH_2 with the additive SrF_2@Gr derived catalyst (MgF_2 + SrH_2)@Gr

The de/rehydrogenation of MgH_2–(MgF_2 + SrH_2)@Gr can be understood based on the results obtained from XRD, TEM, SEM, FTIR and Raman spectroscopic studies conducted in the present investigation.

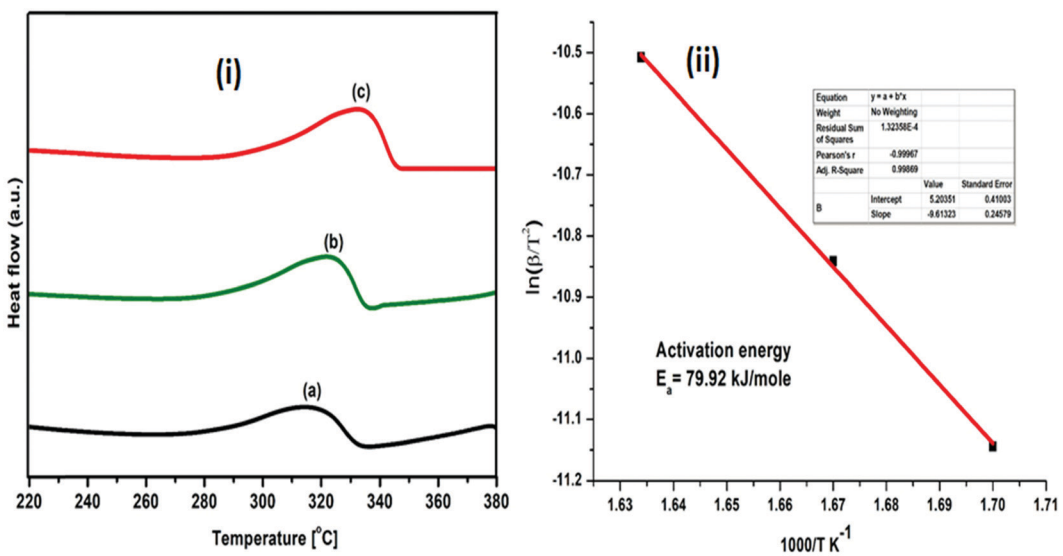

Fig. 10 (i) DSC profiles of (MgF_2 + SrH_2)@Gr catalyzed MgH_2 under heating at (a) 5 °C min^{-1}, (b) 7 °C min^{-1} and (c) 10 °C min^{-1}; (ii) Kissinger plot for evaluating activation energy.

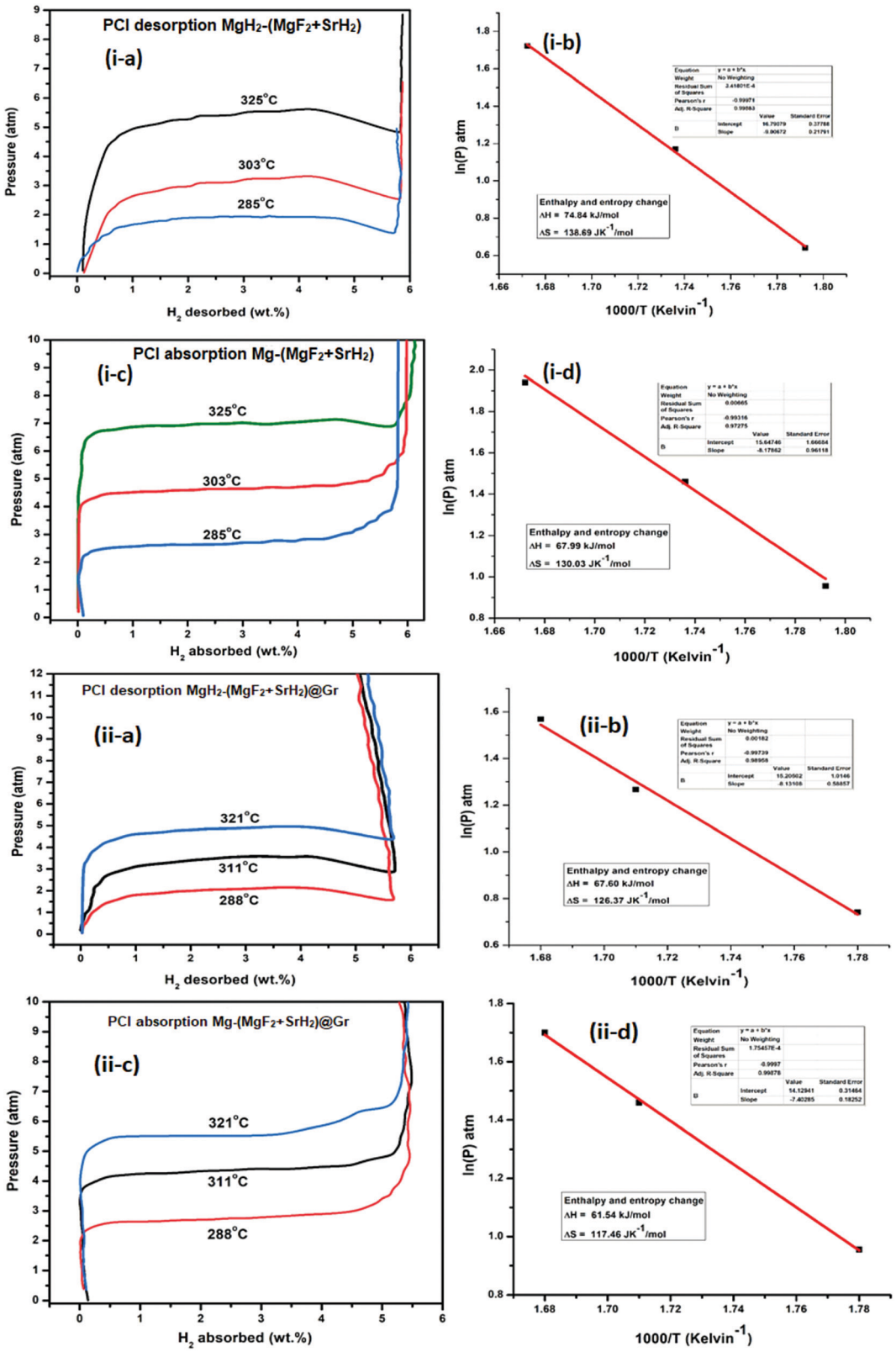

Fig. 11 PCI isotherm of MgH_2 catalysed with: (i-a) PCI desorption at three different temperatures for the MgH_2–(MgF_2 + SrH_2) sample; (i-b) van't Hoff plot for the calculation of change in enthalpy; (i-c) PCI absorption at three different temperatures for the MgH_2–(MgF_2 + SrH_2) sample; (i-d) van't Hoff plot for the calculation of change in enthalpy; (ii-a) PCI desorption at three different temperatures for the MgH_2–(MgF_2 + SrH_2)@Gr sample; (ii-b) van't Hoff plot for the calculation of change in enthalpy; (ii-c) PCI absorption at three different temperatures for the MgH_2–(MgF_2 + SrH_2)@Gr sample; and (ii-d) van't Hoff plot for the calculation of change in enthalpy.

The microstructure of $(MgF_2 + SrH_2)$@Gr catalyzed MgH_2 before and after cycling was analyzed by employing TEM. Fig. 12(a)–(i) show the typical TEM micrographs and the related selected area electron diffraction (SAED) patterns after ball milling and cycling. Also the EDAX analysis of $(MgF_2 + SrH_2)$@Gr catalyzed MgH_2 was conducted (Fig. 12(j)). The EDAX analysis is in keeping with the XRD studies (Fig. 3(c) and Fig. S1(c), ESI†) wherein the presence of MgH_2 and SrF_2 has been found through SAED patterns.

The presence of MgF_2 and SrH_2 even after cycling as evidenced by (Fig. 12(g)–(i)) MgH_2 and SrF_2 shows that these

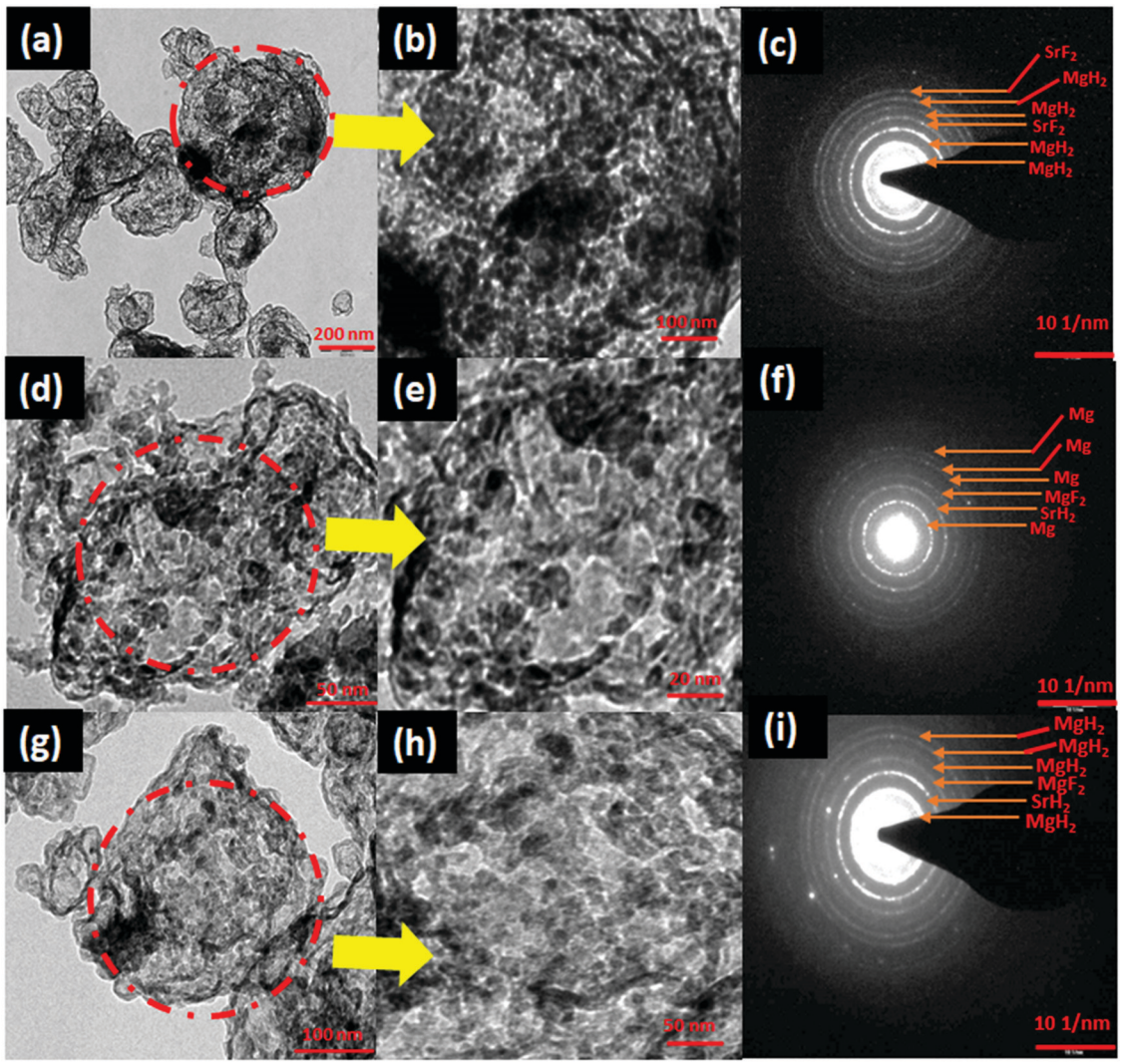

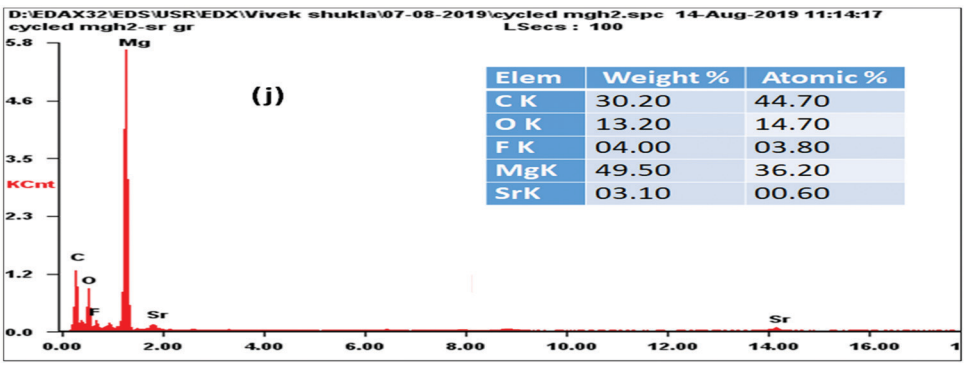

Elem	Weight %	Atomic %
C K	30.20	44.70
O K	13.20	14.70
F K	04.00	03.80
MgK	49.50	36.20
SrK	03.10	00.60

Fig. 12 TEM micrographs of (a and b). MgH_2–SrF_2, (c) SAED pattern of MgH_2–SrF_2, (d and e) Mg–$(MgF_2 + SrH_2)$Gr (1st dehydrogenation), (f) SAED pattern of Mg–$(MgF_2 + SrH_2)$Gr (1st dehydrogenation), (g and h) MgH_2–$(MgF_2 + SrH_2)$@Gr (15 cycles of rehydrogenation), (i) SAED pattern of MgH_2–$(MgF_2 + SrH_2)$@Gr (15 cycles of rehydrogenation), and (j) EDAX spectrum after 15th cycle of rehydrogenation of $(MgF_2 + SrH_2)$Gr catalyzed MgH_2.

catalysts leads to improvements in hydrogen sorption all through. This confirms that they are indeed the catalysts. Also as shown in Fig. 12(g) and Fig. S4(c) (ESI†), there is no agglomeration of MgF_2 and SrH_2. This implies that MgF_2 and SrH_2 are anchored on graphene. Fig. 12(g) and Fig. S4(c) (ESI†) show that MgF_2 and SrH_2 after 15 cycles (Fig. 12(g) or Fig. S4(c), ESI†) are nearly homogeneously dispersed. From the SAED patterns and EDAX analysis of SEM (Fig. 12(j) and Fig. S4(c), ESI†), one can also identify the presence of Mg, Sr, C, and F (some oxygen is also present, which may be due to some oxidation during the transfer of the specimen in the TEM and SEM chambers), showing that the catalysts remain stable even after 15 cycles of de/rehydrogenation. Because of the aforementioned feature, the catalytic activity will not degrade and the storage capacities will not vary with cycling as observed in our investigation (Fig. 8).

It is to be noted that, in the reactivity series,[41] Sr is placed above MgH_2 and hence is highly reactive as compared to Mg. Therefore, there is every possibility of displacement of Mg by Sr. Therefore, the formation of MgF_2 and the associated compound SrH_2 will take place. MgH_2 exhibits an ionic-covalent bond[42] with charge densities as $Mg^{1.509+}$ and $H^{-0.754}$. Khatabi *et al.*[42] have shown that the bonding between Mg and H can be weakened by using a suitable catalyst having active d orbitals. MgF_2 type compounds have active d orbitals in their orbital geometry.[43] MgF_2 is highly ionic owing to the elemental electronegativity difference of 2.67 (Mg: 1.31, F: 3.98), which is higher as compared to the electronegativity difference for MgH_2 which is 0.79 (Mg: 1.31, H: 2.10) being a polar molecule with a high electronegative character and the dominant contribution of the d orbital will readily interact with polar covalent MgH_2, destabilize the Mg–H bond and improve the kinetics. Because of the above reason, MgF_2 will play a dominant role in improving the kinetics. This is in keeping with the known catalytic activity of MgF_2 for hydrogen sorption in MgH_2.[23] In regards to SrH_2 which has a lower elemental electronegativity difference of 0.15 (Sr: 0.95, H: 2.10), it may play a minor role in destabilizing the Mg–H bond. It is known that, if MgH_2 assumes a smaller size in the nanoparticle range, the thermodynamics is improved.[44–46] Fine particles of MgH_2 <5 nm in size were observed in the present studies on mechanical milling. It may thus be considered that SrH_2 plays a major role in improving thermodynamics. This is in conformity with the results obtained in the present investigations. The formation enthalpy of the catalyzed MgH_2 has been found to change from 76 kJ mol^{-1} to 61.54 kJ mol^{-1} (an improvement of 14.46 kJ mol^{-1}). The above discussion suggests that, whereas MgF_2 plays a role in improving the kinetics, SrH_2 helps in the positive tuning of thermodynamics. The two catalysts taken together improve the kinetics and thermodynamics. In regards to the presence of MgF_2 and SrH_2 throughout hydrogen sorption, we have already shown through XRD that these are present even after 15 sorption cycles (Fig. 9). In order to further verify this, we have performed FTIR analyses of the samples at the beginning when MgF_2 and SrH_2 were formed and then after 15 cycles of hydrogen sorption. Fig. S7 (ESI†) presents the representative FTIR spectra. The spectra were analyzed based on the known IR absorption characteristics of the various molecules embodied in the materials. The Mg-H vibration is known to give its signature from 400 to 900 cm^{-1} and 900 to 1300 cm^{-1}, MgF_2 around 1492–1500 cm^{-1} and SrH_2 around 1140 cm^{-1}.[47–49] The typical graphene C–H stretching vibration at 2850 and 2930 cm^{-1} can also be noted.[50] The presence of all these can be clearly seen in the FTIR spectra shown in Fig. S6, ESI.†

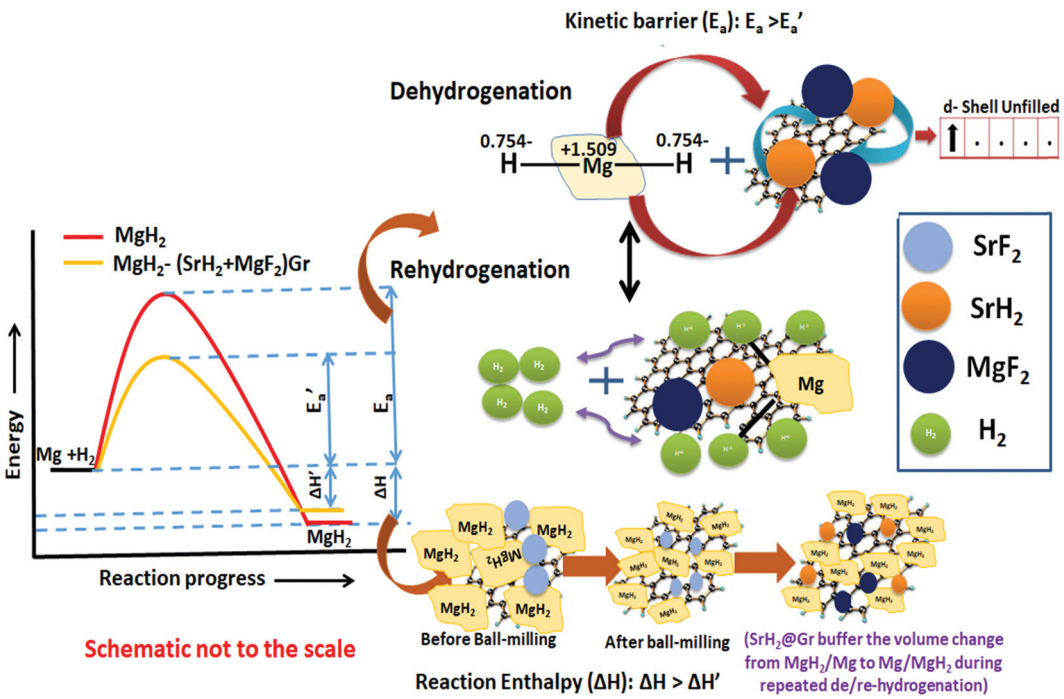

Fig. 13 Schematic diagram of the de/rehydrogenation of MgH_2–(MgF_2 + SrH_2)@Gr.

Recent studies have shown that the hydride catalyst moves from within MgH_2 to the surface during dehydrogenation and *vice versa* during hydrogenation.[44,45] Such movement will buffer the variation of the volume of MgH_2 due to repeated expansion and contraction during de/rehydrogenation. The volume change during repeated de/rehydrogenation is one of the causes for degradation in the cyclic performance of MgH_2. As discussed earlier (Sections 3.1(a) and 3.2(d)), TEM studies reveal that MgF_2 and SrH_2 are anchored on graphene. They do not agglomerate and as outlined earlier this improves the cyclability. The role of graphene in promoting the possible conversion of MgF_2 to MgF_{2-x} and SrH_2 to SrH_{2-x} cannot be ruled out. Thus the enhancement in kinetics, positive tuning of thermodynamics and very good cyclability can be attributed to the synergistic effect between MgF_2, SrH_2 and Gr. This is outlined in the schematic diagram shown in Fig. 13. The simultaneous improvement of all three crucial characteristics, namely, the kinetics, thermodynamics and cyclability, of hydrogen sorption in MgH_2 makes the present investigation different than other studies on fluoride catalyzed MgH_2.

5 Conclusion

The present study deals with the role of one of the most ionic additives SrF_2 in the formation of the catalysts MgF_2 and SrH_2 and their role in the improvement of hydrogen sorption in MgH_2. Besides the additive SrF_2 alone and the resulting catalyst (MgF_2 + SrH_2), their graphene templated versions were synthesized and deployed for hydrogen sorption in MgH_2. It is shown that the catalysts (MgF_2 + SrH_2) and (MgF_2 + SrH_2)@Gr both show better hydrogen sorption characteristics than the presently known best fluoride additive/catalyst NbF_5/(MgF_2 + $NbH_{0.9}$). The catalyst (MgF_2 + SrH_2)@Gr shows very fast hydrogen absorption kinetics of 6.16 wt% in 2 min and desorption kinetics of 6.01 wt% in 15 min in Mg/MgH_2 at 290 °C. The change in desorption enthalpy for (MgF_2 + SrH_2)@Gr catalyzed MgH_2 was found to be 67.60 kJ mol^{-1} (7.42 kJ mol^{-1} lower than the desorption enthalpy of MgH_2–(MgF_2 + SrH_2)). Also the storage capacity of MgH_2 employing the aforementioned catalyst remains 6.10 wt% up to 15 cycles exhibiting excellent cyclability. It has been shown that, whereas MgF_2 plays a major role in improving the kinetics, SrH_2 allows positive tuning of the thermodynamics. All in all, the improvement of the important hydrogen sorption characteristics (kinetics, thermodynamics and cyclability) arises due to the synergistic effect of MgF_2, SrH_2 and Gr.

Conflicts of interest

There are no conflicts to declare.

Acknowledgements

The financial support from the Ministry of New and Renewable Energy (Mission Mode Project on Hydrogen Storage), DST (FIST), SPARC, DRDO, ISRO and the University Grants Commission is thankfully acknowledged. Vivek Shukla would like to thank CSIR New Delhi for providing CSIR-SRF (file no. 09/013(0761)/2018-emr-i).

References

1 M. Momirlan and T. N. Veziroglu, *Renewable Sustainable Energy Rev.*, 2002, **6**, 141–179, DOI: 10.1016/S1364-0321(02)00004-7.
2 S. Singh, A. Bhatnagar, V. Dixit, V. Shukla, M. A. Shaz, A. S. K. Sinha and O. N. Srivastava, *Int. J. Hydrogen Energy*, 2016, **41**, 3561–3570, DOI: 10.1016/j.ijhydene.2015.12.174.
3 S. A. Abbasi and N. Abbasi, *Appl. Energy*, 2000, **65**, 121–144, DOI: 10.1016/S0306-2619(99)00077-X.
4 J. Murray and D. King, *Nature*, 2012, **481**, 433–435, DOI: 10.1038/481433a.
5 D. J. Wuebbles and A. K. Jain, *Fuel Process. Technol.*, 2001, **71**, 99–119, DOI: 10.1016/S0378-3820(01)00139-4.
6 T. Matsuno, K. Maruyam and J. Tsutsui, *Proc. Jpn. Acad., Ser. B*, 2012, **88**, 368–384, DOI: 10.2183/pjab.88.368.
7 T. Searchinger, R. Waite, C. Hanson and J. Ranganathan, *World Resour. Rep.*, 2019, 558. https://www.wri.org/publication/creating-sustainable-food-future?segid=cecb10dd-9466-45e1-a5b8-5693ccfc9cdd.
8 M. Ball and M. Wietschel, The Future of Hydrogen-Opportunities and Challenges, *Int. J. Hydrogen Energy*, 2009, **34**, 615–627, DOI: 10.1016/j.ijhydene.2008.11.014.
9 L. Schlapbach and A. Züttel, *Materials Sustainable Energy*, Co-Published with Macmillan Publishers Ltd, UK, 2010, pp. 265–270, DOI: 10.1142/9789814317665_0038.
10 V. Shukla, A. Bhatnaga, P. K. Soni, A. K. Vishwakarma, M. A. Shaz, T. P. Yadav and O. N. Srivatava, *Phys. Chem. Chem. Phys.*, 2017, **19**, 9444–9456, DOI: 10.1039/C6CP08333A.
11 M. Momirlan and T. Veziroglu, *Int. J. Hydrogen Energy*, 2005, **30**, 795–802, DOI: 10.1016/j.ijhydene.2004.10.011.
12 J. O. Abe, A. P. I. Popoola, E. Ajenifuja and O. M. Popoola, *Int. J. Hydrogen Energy*, 2019, **44**, 15072–15086, DOI: 10.1016/j.ijhydene.2019.04.068.
13 R. R. Shahi, A. Bhatanagar, S. K. Pandey, V. Shukla, T. P. Yadav, M. A. Shaz and O. N. Srivastava, *Int. J. Hydrogen Energy*, 2015, **40**, 11506–11513, DOI: 10.1016/j.ijhydene.2015.03.162.
14 T. Sadhasivam, H. T. Kim, S. Jung, S. H. Roh, J. H. Park and H. Y. Jung, *Renewable Sustainable Energy Rev.*, 2017, **72**, 523–534, DOI: 10.1016/j.rser.2017.01.107.
15 G. Liang, J. Huot, S. Boily, A. Van Neste and R. Schulz, *J. Alloys Compd.*, 1999, **292**, 247–252, DOI: 10.1016/S0925-8388(99)00442-9.
16 S. A. Pighin, B. Coco, H. Troiani, F. J. Castro and G. Urretavizcaya, *Int. J. Hydrogen Energy*, 2018, **43**, 7430–7439, DOI: 10.1016/j.ijhydene.2018.02.151.
17 S. A. Pighin, G. Urretavizcaya and F. J. Castro, *Int. J. Hydrogen Energy*, 2015, **40**, 4585–4596, DOI: 10.1016/j.ijhydene.2015.01.153.
18 R. Floriano, S. Deledda, B. C. Hauback, D. R. Leiva and W. J. Botta, *Int. J. Hydrogen Energy*, 2017, **42**, 6810–6819, DOI: 10.1016/j.ijhydene.2016.11.117.

19 N. Recham, V. V. Bhat, M. Kandavel, L. Aymard, J.-M. Tarascon and A. Rougier, *J. Alloys Compd.*, 2008, **464**, 377–382, DOI: 10.1016/j.jallcom.2007.09.130.
20 I. E. Malka, T. Czujko and J. Bystrzycki, *Int. J. Hydrogen Energy*, 2010, **35**, 1706–1712, DOI: 10.1016/j.ijhydene.2009.12.024.
21 I. E. Malka, M. Pisarek, T. Czujko and J. Bystrzycki., *Int. J. Hydrogen Energy*, 2011, **36**, 12909–12917, DOI: 10.1016/j.ijhydene.2011.07.020.
22 A. Jain, S. Agarwal, S. Kumar, S. Yamaguchi, H. Miyaoka, Y. Kojima and T. Ichikawa, *J. Mater. Chem. A*, 2017, **5**, 15543–15551, DOI: 10.1039/C7TA03081A.
23 P. Jain, V. Dixit, A. Jain, O. N. Srivastava and J. Huot, *Energies*, 2015, **8**, 12546–12556, DOI: 10.3390/en81112330.
24 T. Noritake, M. Aoki, S. Towata, Y. Seno, Y. Hirose and E. Nishibori, *Appl. Phys. Lett.*, 2002, **81**, 2008–2010, DOI: 10.1063/1.1506007.
25 K. Awasthi, R. Kumar, H. Raghubanshi, S. Awasthi, R. Pandey, D. Singh and O. N. Srivastava, *Bull. Mater. Sci.*, 2011, **34**, 607, DOI: 10.1007/s12034-011-0170-9.
26 S. K. Verma, A. Bhatnagar, V. Shukla, P. K. Soni, A. P. Pandey, T. P. Yadav and O. N. Srivastava, *Int. J. Hydrogen Energy*, 2020, **45**, 19516–19530, DOI: 10.1016/j.ijhydene.2020.05.031.
27 S. Singh, A. Bhatnagar, V. Shukla, A. K. Vishwakarma, P. K. Soni, S. K. Verma and O. N. Srivastava, *Int. J. Hydrogen Energy*, 2020, **45**, 774–786, DOI: 10.1016/j.ijhydene.2019.10.204.
28 A. Bhatnagar, S. K. Pandey, A. K. Vishwakarma, S. Singh, V. Shukla, P. K. Soni and O. N. Srivastava, *J. Mater. Chem. A*, 2016, **4**, 14761–14772, DOI: 10.1039/C6TA05998H.
29 A. C. Ferrari, J. C. Meyer, V. Scardaci, C. Casiraghi, M. Lazzeri and F. Mauri, *Phys. Rev. Lett.*, 2006, **97**, 187401, DOI: 10.1103/PhysRevLett.97.187401.
30 N. N. Sulaiman and M. Ismail, *Dalton Trans.*, 2016, **45**, 19380–19388, DOI: 10.1039/C6DT03646E.
31 X. Yang, L. Ji, N. Yan, Z. Sun, X. Lu and L. Zhang, *Dalton Trans.*, 2019, **48**, 12699–12706, DOI: 10.1039/C9DT02084E.
32 S.-A. Jin, J.-H. Shim, Y. Cho and K.-W. Yi, *J. Power Sources*, 2007, **172**, 859–862, DOI: 10.1016/j.jpowsour.2007.04.090.
33 P. K. Soni, A. Bhatnagar, M. A. Shaz and O. N. Srivastava, *Int. J. Hydrogen Energy*, 2017, **42**, 20026–20035, DOI: 10.1016/j.ijhydene.2017.05.233.
34 A. Valentoni, G. Mulas, S. Enzo and S. Garroni, *Phys. Chem. Chem. Phys.*, 2018, **20**, 4100–4108, DOI: 10.1039/C7CP07157D.
35 S. A. Pighin, G. Urretavizcaya and F. J. Castro, *J. Alloys Compd.*, 2017, **708**, 108–114, DOI: 10.1016/j.jallcom.2017.02.297.
36 V. Shukla, A. Bhatnagar, S. K. Pandey, R. R. Shahi, T. P. Yadav, M. A. Shaz and O. N. Srivastava, *Int. J. Hydrogen Energy*, 2015, **40**, 12294–12302, DOI: 10.1016/j.ijhydene.2015.07.039.
37 V. Shukla, A. Bhatnagar, S. Singh, P. K. Soni, S. K. Verma, T. P. Yadav and O. N. Srivastava, *Dalton Trans.*, 2019, **48**, 11391–11403, DOI: 10.1039/C9DT02270H.
38 M. Ismail, *Int. J. Hydrogen Energy*, 2014, **39**, 2567–2574, DOI: 10.1016/j.ijhydene.2013.11.084.
39 S. T. Sabitu, O. Fagbami and A. Goudy, *J. Alloys Compd.*, 2011, **509**, S588–S591, DOI: 10.1016/j.jallcom.2010.11.174.
40 D. Pukazhselvan, N. Nasani, P. Correia, E. Carbo-Argibay, G. Otero-Irurueta, D. G. Stroppa and D. P. Fagg, *J. Power Sources*, 2017, **362**, 174–183, DOI: 10.1016/j.jpowsour.2017.07.032.
41 W. F. Kieffer, *J. Chem. Educ.*, 1950, **27**, 659, DOI: 10.1021/ed027p659.
42 M. El Khatabi, S. Naji, M. Bhihi, A. Benyoussef, A. El Kenz and M. Loulidi, *J. Alloys Compd.*, 2018, **743**, 666–671, DOI: 10.1016/j.jallcom.2017.11.083.
43 L. Seijo, Z. Barandiarán and S. Huzinaga, *J. Chem. Phys.*, 1991, **94**, 3762, DOI: 10.1063/1.459748.
44 A. Bhatnagar, J. K. Johnson, M. A. Shaz and O. N. Srivastava, *J. Phys. Chem. C*, 2018, **122**, 21248–21261, DOI: 10.1021/acs.jpcc.8b07640.
45 J.-S. Youn, D.-T. Phan, C.-M. Park and K.-J. Jeon, *Int. J. Hydrogen Energy*, 2017, **42**, 20120–20124, DOI: 10.1016/j.ijhydene.2017.06.130.
46 R. R. Shahi, R. K. Mishra, V. Shukla, A. Bhatnagar and O. N. Srivastava, *Int. J. Hydrogen Energy*, 2017, **42**, 29350–29359, DOI: 10.1016/j.ijhydene.2017.09.174.
47 X. Wang and L. Andrews, *J. Phys. Chem. A*, 2004, **108**, 11511–11520, DOI: 10.1021/jp046410h.
48 A. Lashgari, S. Ghamami, M. Golzani, G. Salgado-Morán, D. Glossman-Mitnik, L. Gerli-Candia and B. Abdolmaleki, *J. Chil. Chem. Soc.*, 2016, **61**, 3201–3205, DOI: 10.4067/S0717-97072016000400010.
49 U. Magg, H. Birk and H. Jones, *Chem. Phys. Lett.*, 1988, **14**, 263–266, DOI: 10.1016/0009-2614(88)85286-2.
50 M. Coroş, F. Pogacean, T. Ioan-Alexandru, M. Dan, C. Grosan and I.-O. Pana, *Phys. E*, 2020, **119**, 113971, DOI: 10.1016/j.physe.2020.113971.